Received: 5 May 2022 | Revised: 16 August 2022 | Accepted: 20 August 2022

DOI: 10.1002/er.8696

SPECIAL ISSUE RESEARCH ARTICLE

INTERNATIONAL JOURNAL OF ENERGY RESEARCH WILEY

Electrooxidation of methanol on Ag, AgNi, and AgCo catalysts prepared by combustion synthesis technique

Afdhal Yuda[1] | **Anand Kumar**[1] | **Ibrahim Abu Reesh**[1] | **Christopher K. Russell**[2] | **Jeffrey T. Miller**[2] | **Mohammed Ali Saleh Saad**[1,3] | **Mohammed J. Al-Marri**[1]

[1]Department of Chemical Engineering, College of Engineering, Qatar University, Doha, Qatar

[2]Davidson School of Chemical Engineering, Purdue University, West Lafayette, Indiana, USA

[3]Gas Processing Center, College of Engineering, Qatar University, Doha, Qatar

Correspondence
Anand Kumar, Department of Chemical Engineering, College of Engineering, Qatar University, Doha, P O Box 2713, Qatar.
Email: akumar@qu.edu.qa

Funding information
Qatar National Research Fund, Grant/Award Numbers: NPRP13S-0109-200029, NPRP8-509-2-209; U.S. Department of Energy, Office of Science, and Office of Basic Energy Sciences, Grant/Award Number: DE-AC02-06CH11357

Summary

Herein, we report the synthesis of silver-based electrocatalysts (Ag/C, AgCo/C, and AgNi/C) using solution combustion method and their performance towards methanol oxidation reaction. Detailed structural and microscopic analysis confirmed the formation of graphitic carbon, synthesis of crystalline phases with high porosity in all the three electrocatalysts. X-ray photoelectron spectroscopic (XPS) analysis showed a high concentration of Ag_2O (or Ag^{+}) on AgNi/C, whereas AgCo/C exhibited a high concentration AgO (or Ag^{2+}) on the surface. XPS analysis on C 1s confirmed the highest concentrations of the sp^2 hybridized C—C bond on Ag/C, C═O on AgNi/C, and O—C═O bond on AgCo/C, respectively. The X-ray absorption spectroscopy (XAS) analysis on Ag edge showed a similarity in the bond lengths in AgCo and AgNi samples to that of bulk silver, that has a bond length of 2.89 Å, with only silver-silver scattering and the absence of a different or a nonsilver metal in the nanoparticles. This indicates that there is no Ag-M alloying. Nonetheless, a significant difference in particle sizes was observed, with 2.5 and 6 nm, respectively for AgNi and AgCo. Methanol electrooxidation experiments performed on the electrocatalysts indicated AgNi/C to show better performance in comparison to AgCo/C and Ag/C. Anodic polarization curves obtained from linear sweep voltammetry (LSV) measurements demonstrated a superior performance of AgNi/C with an onset potential of 0.41 V. In addition, 20 h chronoamperometry experiment also confirmed a sustained superior performance of AgNi/C catalyst, which could be due to smaller particle size and stabilization of Ag+ on the surface of the catalyst.

KEYWORDS
methanol electrooxidation, silver based catalysts, solution combustion synthesis

1 | INTRODUCTION

The widespread awareness of the danger of harmful emissions from the use of fossil fuels has contributed to the need to find alternative energy sources that are more environmentally friendly. The fuel cell is one such alternative that has recently become a focus of many studies. It has the ability to generate energy with fewer or no harmful emissions for a wide range of technological applications such as mobile phones, laptops, and even transportations. Direct methanol fuel cell (DMFC) in particular is a fuel cell which has been intensively studied due to their attractive characteristics that include low operating temperature, high energy density, environmental friendliness and efficient energy conversion property.[1,2] However, for their practical operations, electrocatalysts are required on each of the electrodes (anode and cathode) to efficiently drive the anodic and cathodic reactions. For large-scale applications, a challenge arises in finding electrocatalysts that are not only of low cost, but that can also actively drive the reactions in fuel cells. Precious metals, such as platinum, are effective in promoting both anodic and cathodic reactions, including methanol oxidation reactions (MOR).[3] However, because platinum is scarce, expensive, and sensitive to poisoning by carbon monoxide at the anode, its usage for large-scale applications has been significantly restricted.[4-12] Hence, the scientific community is posed with a challenge of developing a suitable and efficient catalyst for the widespread use of DMFCs.

Alternative materials, such as gold, palladium, silver, and rhodium nanoparticles (NPs), on the other hand, are relatively abundant, demonstrate excellent catalytic activity and have a tendency to withstand CO intermediate poisoning during MOR.[13-16] However, due to the metal NPs' high surface energy and small size, they tend to agglomerate during reaction causing gradual decrease in activity over a period of time. Such occurrences can be prevented by anchoring the metal NPs onto carrier materials, such as nanostructured carbons, with high thermal conductivity characteristic[17,18] on which the growth of metal nanoparticles could be suppressed to achieve high stability of small particles through the heat sink effect.[19,20] Furthermore, carbon support with high surface area helps in improving the usage of the overall electrocatalysts through activity escalation by improving the surface charge transfer effect. Examples of carbon support that could be used include carbon black, carbon nanotubes, graphene, and carbon nanofiber, and they are also capable of demonstrating good electrical conductivity as well as stability.[21]

One of the metals that has been studied to demonstrate promising results for methanol oxidation is silver, which is capable of showing long-term stability as well as better selectivity of product.[22] Roshan et al. synthesized an electrode material consisting of silver in the form $CuAg/Cu_2O$ nanoparticles on two-dimensional C—N nanosheets surface.[23] The decoration of $CuAg/Cu_2O$ on C—N was achieved by galvanic method in which the sacrificial Cu and Cu_2O atoms were substituted by atoms of Ag. It was determined that the C—N/$CuAg/Cu_2O$ hybrid catalyst displayed improved performance when compared to C—N/Cu/Cu_2O electrocatalyst for methanol oxidation as well as better selectivity for the conversion of CO_2 into formate. The enhanced performance of CuAg catalyst during MOR could be because the silver surface forms weak oxygen bond while copper forms strong bond during oxidation reactions. The better preference in converting CO_2 to formate, on the other hand, could be ascribed to the suppression of side reaction, in particular hydrogen evolution. The reason may also be the generation of strain in CuAg alloy, which may prefer a reduced hydrogen coverage that minimizes copper's oxophilicity.

The usage of nickel as an electrocatalyst material is well known because of its surface oxidation properties. It has commonly been used to promote anodic and cathodic reactions in organic synthesis as well as in water electrolysis.[24-27] The performance of nickel-containing electrocatalysts toward alcohols oxidation has also been studied in the past.[28] A study performed by Taraszewska and Roslonek reported the effectiveness of a glassy carbon/$Ni(OH)_2$ modified electrode toward methanol oxidation.[29] It was observed that most oxidizable organic compounds oxidized at the same potential value which matched exactly with the value at which nickel anode surface becomes oxidized.[28-32] In another study by Van Effen and Evans, which involved the oxidation of ethanol in a KOH solution, there was a formation of higher valence nickel oxide that behaved as a chemical oxidizing agent.[33] Such occurrence was confirmed by cyclic voltammetry (CV) and alternating current impedance measurement analysis. CV analysis enabled the determination of the existence of a mediation process that involved higher oxides and organic molecules. Cobalt is another transition metal well-known for its catalytic activity for various chemical reactions. However, it is not generally used as a primary electrocatalyst material because of its low electrocatalytic performance. It is instead used as a cocatalyst with platinum for instance, to help resist CO poisoning of the active sites. Oxides of cobalt (Co_3O_4 and CoO) as a catalyst material have also become popular due to their remarkable intrinsic properties; including structural flexibility, adjustable chemical properties, and higher activity.[34] These enhanced performances are ascribed to the existence of many electroactive surface sites and tailored electronic structure attained by applying cost-effective

and versatile synthesis techniques. Pt-Co alloys have been reported to possess great CO-resistivity characteristic.[35,36] It is also capable of showing excellent electrochemical self-stability as demonstrated by Hidai and team.[37] They evaluated the accelerated durability of platinum-cobalt alloy through the application of potential cycling between a value of 0.6 and 1.0 V. They observed that after 10 000 cycles, the electrocatalyst displayed less electrochemically active surface area (ECSA) decay as well as particle growth than the platinum catalyst. This suggests that combining cobalt to the platinum crystal lattice can effectively restrict the Ostwald ripening effect because of the growth limit behavior,[29] and/or the restriction of platinum oxides formation.[28,30] Furthermore, through cobalt addition, more efficient initiation of methanol dehydrogenation could take place that results in a relatively better catalytic performance toward MOR in comparison to using platinum alone.[31] Ashok et al. reported the synthesis of cobalt-based electrocatalyst for MOR in alkaline medium in the form of hierarchical Co_9S_8 nanowires trapped in nitrogen-doped carbon nanotubes (N,S-Co@CNT) attained from melamine.[38] They performed material characterization which established that adding sulfur during pyrolysis improved the surface area, lattice defect, and pore size. Furthermore, morphology changes from hemispherical particles to nanowires was observed, that further enhanced the electrochemical characteristics. The methanol oxidation electrocatalytic results confirmed that N,S-Co@CNT displayed a significantly greater current density and a considerably lower onset potential than Co@CNT. Other than enhanced activity, N,S-Co@CNT also demonstrated a better stability that could be explained by the unique hierarchical structure and surface properties. Roshan et al. studied the use of cobalt by synthesizing a mixed oxide nanosheet of Co_3O_4/CuO through solution combustion synthesis for MOR.[39] The performance of the synthesized electrocatalyst surpassed that of catalysts made of individual CuO and Co_3O_4 nanosheets. During MOR (0.5 M) a mass activity of 12 mA g^{-1} was shown by the mixed Co_3O_4/CuO nanosheet at 0.627 V (vs Ag/AgCl), which is 2.4 times greater than that of Co_3O_4 (mass activity of 5 mA g^{-1}) and four times greater than that of CuO nanosheet (mass activity of 3 mA g^{-1}). Furthermore, a more intense peak of methanol oxidation at 0.62 V (vs Ag/AgCl) was observed than those catalysts made of individual CuO and Co_3O_4. The enhanced efficiency could be because of the existence of abundant active sites on the nanosheet edges, surface defects, and the presence of micropores. Based on an analysis by Sun and team, sites of atoms at the nanosheet edges possess unsaturated coordination in addition to dangling bonds which results in reduced activation energy barrier and improved stability of the reaction intermediates.[40] Hence, the nanosheets' edge atoms that are more exposed to reactant molecules act as active sites. Surface defects also exists along the micropores in nanosheets that enable reactants diffusion and assist in product formation. Atoms present in the micropores are, in addition, less coordinated and more exposed to reactants, and therefore these can also be regarded as active sites. The surface area of the nanosheet was large with the porous characteristic of the surface, and these micropores, including the surfaces' defects and edges of the nanosheets, may act as the active sites in the hybrid electrocatalyst. Moreover, Co_3O_4 and CuO interfaces (intercalation of crystal planes) are also likely to be rich sources of active sites and this could explain the superior activity of the synthesized Co_3O_4/CuO nanosheet electrocatalyst.

In this paper, we report the MOR performance of three types of electrocatalysts synthesized using the solution combustion synthesis method, which include Ag, AgNi, and AgCo. The material systems were selected based on the results of studies that developed high-performing electrocatalysts based on the utilization of silver, nickel, and cobalt as cited above. Using silver helps develop electrocatalysts that can achieve long-term stability and better product selectivity. Making use of nickel in the material system takes advantage of its surface oxidation properties and having cobalt as a co-metal can promote resistance against CO poisoning of the active sites as well as form more electroactive surface sites for MOR. Glycine was used as fuel during combustion synthesis, and a fixed ratio of glycine-to-fuel and silver-to-nickel or silver-to-cobalt were maintained during the synthesis of the catalysts which were tested for methanol electrooxidation. Experimental results show that the silver in presence of Ni and Co perform relatively better than that of silver nanoparticles (NPs) by itself. The details of experimental methods; including synthesis conditions, structural characterizations and electrochemical methods used in this study are provided in the following section.

2 | EXPERIMENTAL

2.1 | Chemicals

Silver nitrate ($AgNO_3$, 99%), cobalt(II) nitrate hexahydrate ($Co(NO_3)_2{\cdot}6H_2O$, 98 %), nickel(II) nitrate hexahydrate ($Ni(NO_3)_2{\cdot}6H_2O$, 97%), glycine (99.7%), isopropyl alcohol, and Nafion solution (5 wt.%) reagents were purchased from Sigma-Aldrich. Carbon black (VXC72) and Potassium hydroxide (KOH, 85%) were purchased from

Cabot Corporation and Riedel-de Haen, respectively. Methanol (CH_3OH, 99.8%) was purchased from BDH, AnalaR. Ultrapure water (Millipore, 18.2 MΩ cm) was utilized during the whole study. All the reagents were used without any further purification.

2.2 | Synthesis

Weighed quantities of $AgNO_3$, $Ni(NO_3)_2{\cdot}6H_2O$ and glycine were poured into a 250 ml beaker and were mixed with 20 ml of deionized water (DIW). The beaker was then kept in a sonic vibrator bath to achieve a homogenous solution and the beaker filled with the reagents were then placed on a hot plate with a temperature of 250°C. As time passes, evaporation of the solution occurred and approximately, after 30 minutes, the catalyst materials were obtained as a result of combustion reaction by self-ignition that took place in the beaker. Afterwards, the resulting material was ground with the help of a pestle and a mortar, and sieved to achieve particles of uniform size. The preparation of the catalyst containing silver and cobalt were also performed using the same method. The molar ratios of the metal precursors in Ag-M samples were maintained at 1:1. Addition of glycine fuel to the mixture was determined based on a glycine to oxidizer ratio (ϕ) as formulated in literatures.[31,32,38,41,42] In the three electrocatalyst samples the reactant ratios (Ag: co-metal: glycine [ϕ]) were 1:1:1.5 for both AgNi/C and AgCo/C samples, and 1:0:1.5 for Ag/C. Afterwards, 40 wt.% of the synthesized catalyst powder was added to 60 wt.% carbon support material to obtain the carbon supported electrocatalysts. Each catalyst powders were then dispersed in 7 ml DIW in a beaker of 50 ml in volume and heated to 125°C until all the water is evaporated before leaving the samples to fully dry. The synthesis schematic is shown in Figure 1.

2.3 | Characterization techniques

X-ray diffraction (XRD) characterization studies were performed on the synthesized samples using a powder X-ray diffractometer (Rigaku MiniFlexII Desktop, Cu-Kα radiation [$\lambda = 1.54056$ Å]). The JCPDS card number of the standard pattern of Ag, Ni, and Co_3O_4 were 98-006-4997, 98-016-3354, and 98-004-2684, respectively. Transmission electron microscopy (TEM, TECNAI G^2, F20 FEI) analysis was completed for morphological study of the samples. The method involves ultrasonically dispersing a small quantity of the sample in ethanol after which a few drops of the solution was placed onto a carbon-coated Cu-grids and then left to dry in ambient temperature. An energy dispersive X-ray spectroscopy analyzer coupled to a field-emission scanning electron microscope (SEM; Nova Nano 450, FEI) was utilized to determine the elemental compositions and particle morphology in the samples. Analysis of the oxidation state of the elements in the samples was performed using X-ray photoelectron spectroscopy (XPS, Kratos AXIS Ultra DLD) and the reported binding energies (BEs) in the XPS data were calibrated with respect to C 1s at 284.8 eV. Performance of X-ray absorption spectroscopy (XAS) experiments were completed at the 10-BM-B beamline at the Advanced Photon Source (APS), Argonne National Laboratory in the transmission mode, using an energy resolution of 0.3 eV and edge energy precision of more than 0.1 eV. The experiment involved loading the sample in a 6-channel holder placed in a quartz tube capped with Ultra Torr fittings to secure the cell from the atmosphere. Scanning of the samples was then performed at room temperature as received in fast scan mode at the Ag K-edge (edge energy of 25.514 keV). Each measurement was accompanied by simultaneous foil measurement in a third ion chamber to perform internal energy calibration. WinXAS 3.1 software was utilized to process all the data using standard techniques.

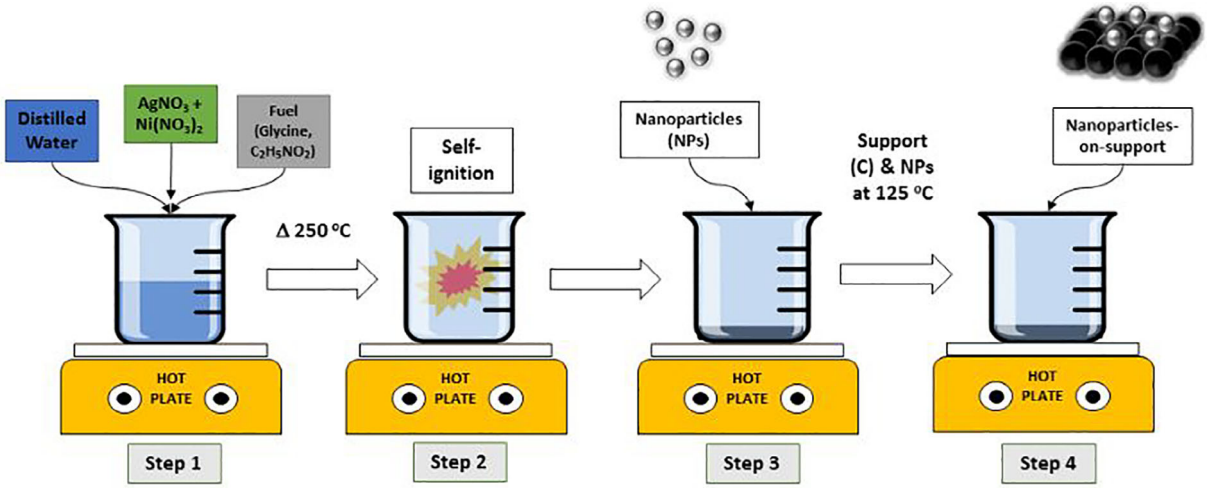

FIGURE 1 A schematic representation of the solution combustion synthesis technique

2.4 | Electrode procedures

Analysis of the electrocatalytic performance of Ag/C, AgCo/C, and AgNi/C toward MOR was performed with a three-cell PINE electrode bipotentiostat (Wave Driver 20) in a basic medium. The ink of the working electrode was prepared by mixing 5 mg of the catalyst with 300 µl of isopropyl alcohol and 30 µl of Nafion (a binder) using an ultrasonicator for 10 minutes. An ink was then formed, from which 5 µl was taken and dropped carefully onto a 5 mm glassy carbon disc supported by a Teflon mounting that was then left to dry at ambient condition. A platinum coil supported by an epoxy rod was used as a counter electrode while a 4 M KCl-saturated Ag/AgCl was used as a reference electrode. Before starting with the electrochemical measurements, the basic solution of 1 M KOH was fully purged with nitrogen to remove any unwanted gaseous impurities that may be present in the electrolyte. The pretreatment was performed on the working electrode to ensure that the surface of the electrode is stable and this involved conducting 100 oxidation-reduction cycles at 500 mV s^{-1} scan rate. The MOR study was performed in a solution containing 1 M KOH and 1 M methanol (CH_3OH) with a potential value that ranges from −0.6 V and +0.6 V (vs Ag/AgCl) at 10 mV s^{-1} that was purged with nitrogen initially for a duration of 30 minutes. Linear sweep voltammetry (LSV) was also performed with potentials between the values of 0 V and +0.8 V (vs Ag/AgCl) at 5 mV s^{-1} scan rate. A potential window of 0 to 0.8 V was chosen for LSV in order to clearly determine the onset potential of each catalyst and to better observe the pattern of the methanol oxidation reaction for each of them. A potential window of −0.6 to 0.6 V was selected for CV, on the other hand, to examine the reduction (negative potential range) and oxidation (positive potential range) behavior of each catalyst. The potential window selected for CV was also based on the expected oxidation and reduction potential for the compounds. LSV, cyclic voltammetry (CV) as well as chronoamperometry (CA) were all conducted to analyze the electrocatalytic performance of the three synthesized samples toward MOR. The measured current values were converted to current density by dividing them with the area of the working electrode (0.197 cm^2). All analysis conducted were performed at room temperature of 25°C.

3 | RESULTS AND DISCUSSION

The XRD pattern of the prepared samples of Ag/C, AgNi/C, and AgCo/C is shown in Figure 2. A common characteristic peak noticeable at 26.1° for AgNi/C and AgCo/C, signifies the presence of (002) crystal plane of graphitic carbon in carbon nanotubes (CNTs). There are four peaks

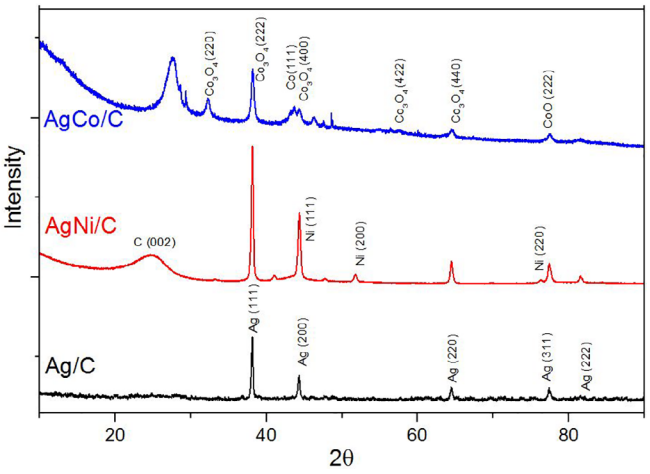

FIGURE 2 X-ray diffraction analysis of combustion synthesized Ag-M catalysts

common to all the three samples at $2\theta = 38.2°$, 44.3°, 64.6°, and 77.6° and correspond to silver metal (hkl) planes values of (111), (200), (220), and (311) planes of silver. The XRD analysis has thus confirmed that the as-synthesized samples consist of silver nanoparticles that have face-centered cubic (fcc) crystal structure. There are also additional peaks at 31.28°, 38.2°, 44.3°, 59.21°, 65.32° displayed by the AgCo/C catalysts that correspond to the diffraction pattern of cubic Co_3O_4,[41,43] where some peaks are close to Ag and may have overlapped. With regards to the XRD pattern for AgNi/C there are diffraction peaks located at 2θ values of 45.8°, 51.8°, and 79° that correspond to the (111), (200), and (220) crystal planes of the face-centered cubic nickel particles, respectively. Furthermore, the low intensity peaks at 2θ values of 42.4°, 44.3°, 46.4°, 53.2°, and 69.1° correspond to the (010), (002), (011), (012), and (110) planes signifying the hexagonal closed packed (hcp) nickel structure.[42,44,45] Looking closely at the peaks of Ag(111) planes for the three samples, there is a shift in the value of 2θ to higher values as displayed by AgNi/C and AgCo/C electrocatalysts. The reason for this shift could be because of either the presence of lattice strain or changes in the chemical composition as a result of formation of the solid solution. When there is a replacement of an atom in a unit cell with another atom, for example, in case of doping, the periodicity undergoes a rearrangement that modifies the cell parameters and further generates a shift in diffraction peaks. Relatively greater displacement is observed for AgCo/C that signifies an improved combination of silver and cobalt atoms to produce alloys that behave as transition zones lead in to the formation of bimetal.[46-48]

Figure 3 shows the SEM microimages of the 3 Ag-based electrocatalysts resulting from the synthesis method implemented that leads to various structural and physical changes. Similarities in their microstructures

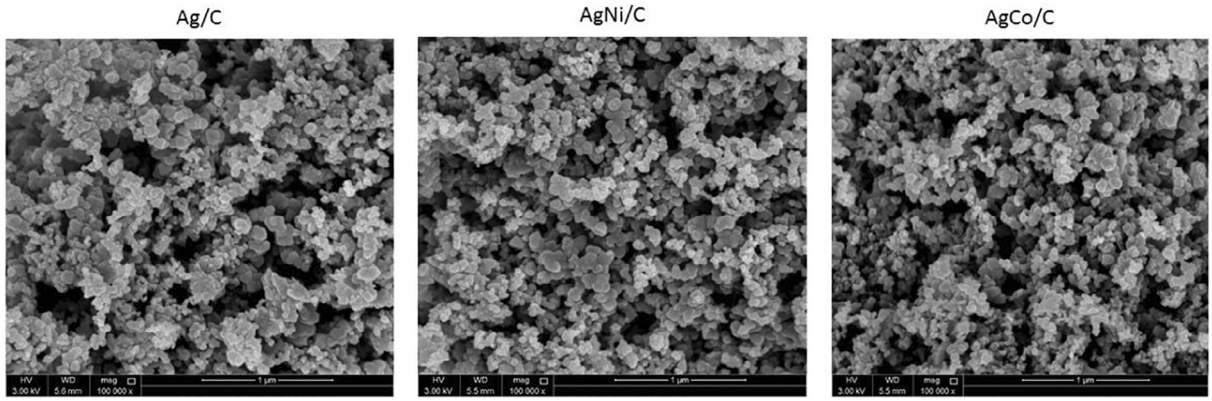

FIGURE 3 Scanning electron microscope analysis of the catalysts Ag/C, AgNi/C and AgCo/C; scale bar = 1 μm

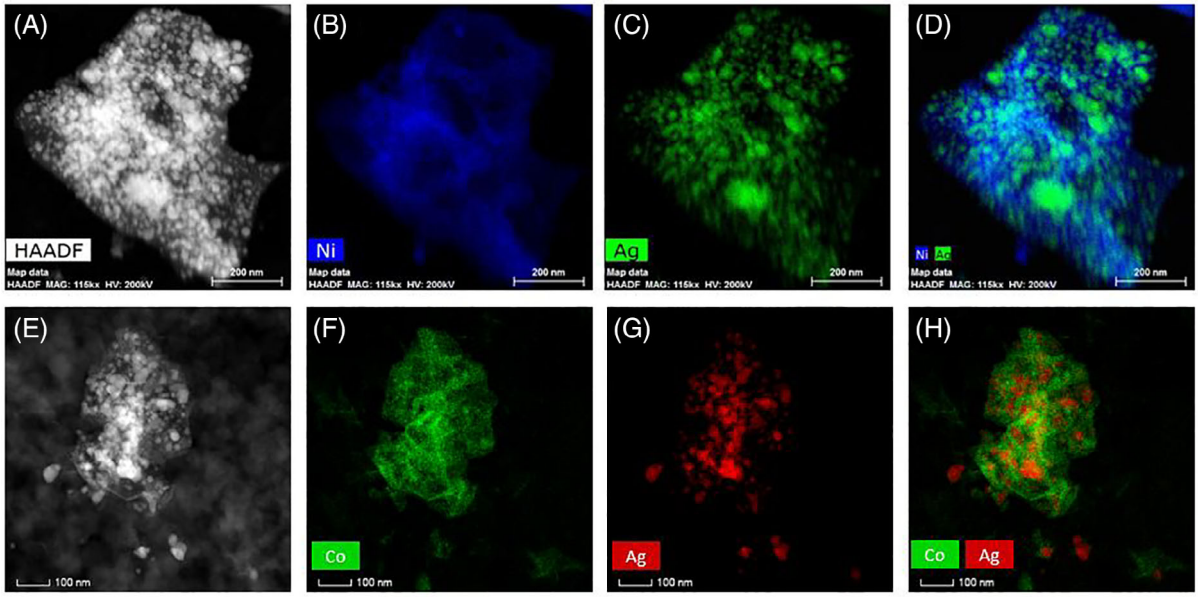

FIGURE 4 HAADF and elemental mapping in (A-D) AgNi/C with scale bar = 200 mn, and (E-H) AgCo/C with scale bar = 100 nm; showing the distribution of elements

can be observed; especially in nanoparticles size distributions and morphological arrangements. Another similarity that could be observed is the existence of well-porous structure on the catalyst surface that is formed as a result of gas evolution during the synthesis process. With such characteristic, the electrocatalysts are expected to have increased surface area that can contribute to improved performance for electrochemical applications.[43,49] In Ag/C, larger clusters can be identified in addition to a distribution of smaller particles. The microstructures presented by both AgNi/C and AgCo/C are quite similar in which fewer larger clusters are observed and the smaller particles are relatively widely distributed, which further influenced the creation of more porous surfaces. Visual inspection is insufficient for elemental identification, and it is necessary to perform further high-resolution analysis. EDX analysis indicated the achievement of targeted elemental ratio in Ag-M with equal proportions of Ag and Ni or Co.

The TEM images with phase mapping of elements in AgNi/C and AgCo/C are shown in Figure 4, and the distribution of different elements in each catalyst could be distinguished. Looking at Figure 4A-D of AgNi/C, several silver nanoparticles (green) of varying sizes are seen to be distributed over larger particles of nickel (blue). The image of AgCo/C (Figure 4E-H), also showed larger particles of cobalt (green) covered the silver nanoparticles. This could be related to the sequence of formation of silver and cobalt or nickel particles during the synthesis process, in which the cobalt or nickel particles are formed first, followed by synthesis of silver particles over the presynthesized cobalt or nickel. This sequence is

correlated with the order of decomposition temperature of the precursors, where cobalt nitrate decomposes earlier than silver nitrate.[43]

Figure 5A shows the XPS spectrum of the three electrocatalysts with two characteristic peaks at approximately 368.4 and 374.4 eV that corresponds to metallic silver Ag $3d_{5/2}$ and Ag $3d_{3/2}$, respectively. Comparing the peak profile of AgNi/C and AgCo/C to that of Ag/C, a shift can be observed in the Ag 3d spectrum of AgCo/C and AgNi/C to a higher value of binding energy. This shift is an indicative of charge transfer taking place between silver and the co-metals, and a strong electronic bonding between the two elements on the surface. As a result, there is an improvement in the surface alloying of the two metals in the AgCo/C and AgNi/C electrocatalysts. Figure 5B-D shows the deconvolution of each spectrum with various peaks that signify the existence of silver in different oxidation states (Ag_2O and AgO indicated as peaks I and III, and II and IV, respectively).[50] Normalized area of each peak was also determined to compare the concentration of various oxidation states. Comparison of the normalized area of peak I, signifying Ag_2O (or Ag^+) of the catalysts, the AgNi/C displays the highest normalized area of 52 units. This is then followed in descending order by AgCo/C (normalized area of 6 units) and Ag/C (normalized area of 4 units). When normalized areas of peak II (signifying AgO or Ag^{2+}) of the catalysts are compared, it was determined that AgCo/C demonstrated the greatest normalized area of 55 units. Ag/C, on the other hand, showed a normalized area value of 28 units and AgNi/C displayed the lowest peak II normalized area of 6 units. The coupling of oxide with silver could be explained by oxygen originating from cobalt oxide in the case of AgCo/C and nickel oxide in the case of AgNi/C, and when alloying takes place the oxygen in nickel oxide and cobalt oxide is substituted with silver. It is also possible that silver is oxidized during the synthesis process, and it could be the case in Ag/C as its Ag 3d spectrum also showed silver in various oxidation states.

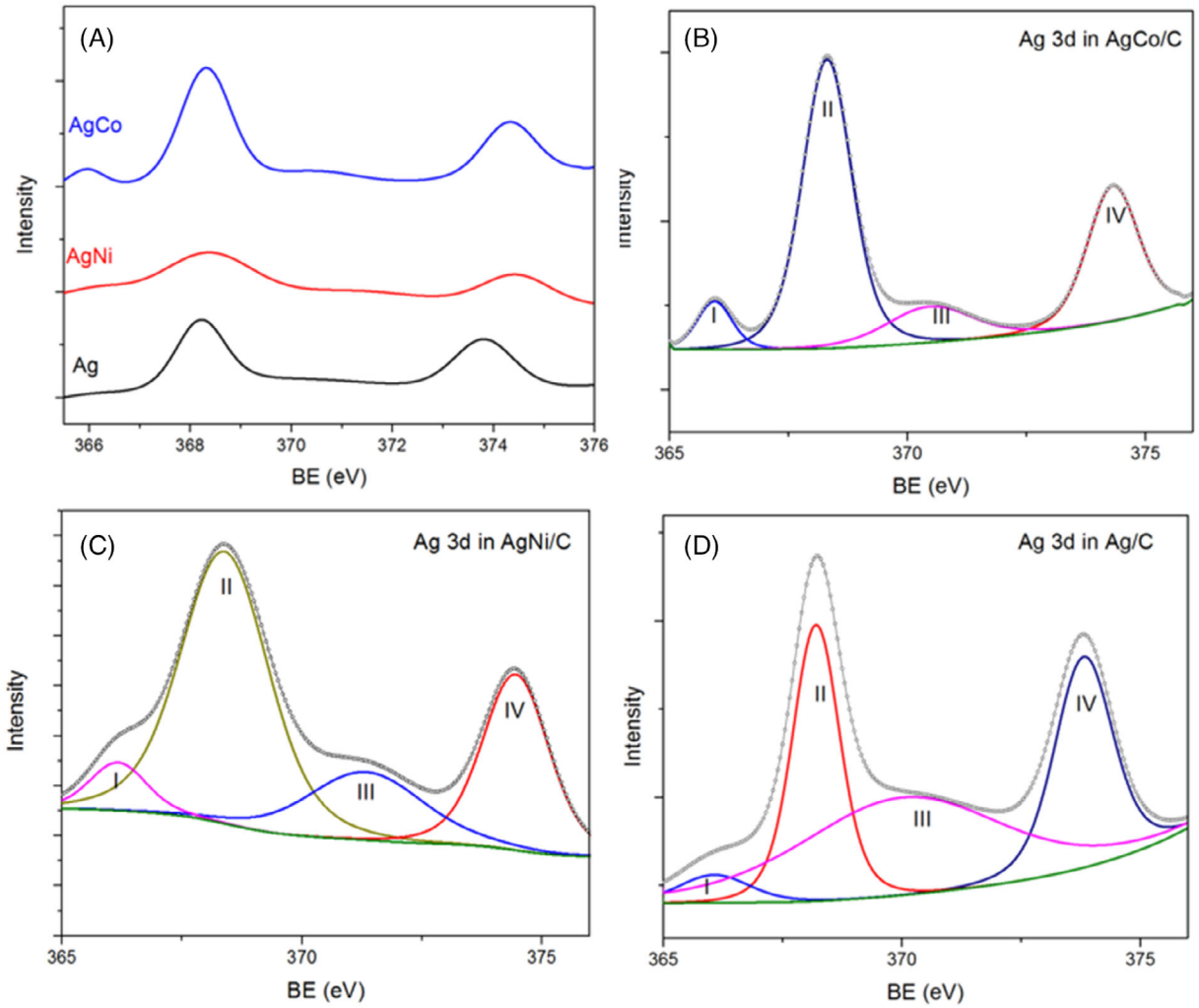

FIGURE 5 XPS spectrum at Ag-3d edge, (A) comparison of samples, (B) AgCo/C, (C) AgNi/C, (D) Ag/C

The Ni 2p spectrum of AgNi/C electrocatalyst is given in Figure 6A that consists of two spin orbital doublet centered at approximately 856.3 and 874 eV and correspond to Ni $2p_{3/2}$ and Ni $2p_{1/2}$ orbitals, respectively. Within each peak, the deconvolution profile indicates the presence of two subpeaks that represent satellite peaks (displayed as peak II and IV) and nickel as NiO (displayed as peak I and III). As indicated by XRD, the bulk of nickel is in metallic form; however, XPS clearly indicates the presence of Ni^{2+} on the surface of the catalyst. Figure 6B displays the Co 2p spectrum of AgCo/C electrocatalyst that indicates two relatively stronger peaks at approximately 782 eV (for Co $2p_{3/2}$) and 797.1 eV (for Co $2p_{1/2}$). In the deconvolution profile of the Co 2p the existence of Co^{3+} (displayed as peaks I and IV) and Co^{2+} (displayed as peaks II and V) are also confirmed. These are characteristic peaks of cobalt oxides that could also be present in the electrocatalyst. Furthermore, satellite peaks could also be observed in the deconvolution profile next to the main peak, assigned to the spin orbital of Co^{2+} (displayed as peaks III and VI). These results confirm the presence of nickel and cobalt in their various oxidation states as Ni^{2+}, Co^{2+}, and Co^{3+} as they co-exist with silver in AgNi/C and AgCo/C electrocatalysts.

The C 1s XPS profiles of the three electrocatalysts were extensively evaluated as shown in Figure 7A with peaks that could originate from carbon atoms being bonded in different configuration. Figure 7B-D shows the deconvolution profiles of the AgCo/C, AgNi/C, and Ag/C, respectively, and they confirm the various carbon atom-bonding configurations. It can be observed that the deconvolution profiles consist of five main characteristic peaks at approximately 284.4 (peak I), 285 (peak II), 286.5 (peak III), 289.5 (peak IV), and 292 eV (peak V) that are assigned to the sp^2 hybridized C—C bond on the graphitic honeycomb structured lattice (sp^2 C—C), alkoxy/epoxy form (C—O, or C—S and C—N), C═O, O—C═O bond formation, and pi-pi* (graphitic shakeup satellite), respectively. Normalized areas of the various peaks were also determined for the electrocatalysts, which established the normalized area of peak I of Ag/C (value of 38 units) to be greater than that of AgNi/C and AgCo/C (value of 33 units and 34 units, respectively). Furthermore, comparison of the normalized areas of peak II of the catalysts demonstrated Ag/C being with the highest normalized area of 40 units, while AgNi/C and AgCo/C displayed relatively lower value of 30 units and 27 units, respectively. The normalized areas of peak III for all the samples, however, are approximately the same, with AgNi/C being slightly higher (value of 17 units) than the values determined for Ag/C (value of 15 units) and AgCo/C (value of 16 units). Analysis of the normalized areas of peak IV deduced that AgCo/C is more dominant (value of 16 units) than that of Ag/C (value of 8 units) and AgNi/C (value of 10 units). In addition, study of the data of the normalized areas of peak V of the various electrocatalysts showed the absence of pi-pi* in Ag/C and relatively smaller values of normalized area for AgNi/C (value of 10 units) and AgCo/C (value of 7 units).

While the XPS analysis indicate the oxidation states and alloying in Ag-M on the surface, XAS analysis on the Ag edge was conducted to understand the bulk structure, Ag-M alloying, interatomic distances and coordination numbers. Results on XANES regions for AgCo/C and AgNi/C are the same as that of silver foil and no remarkable differences are observed (Figure 8A Ag-foil and AgCo are shown). This gives an indication of the similarity of the particles to the bulk silver, which also means

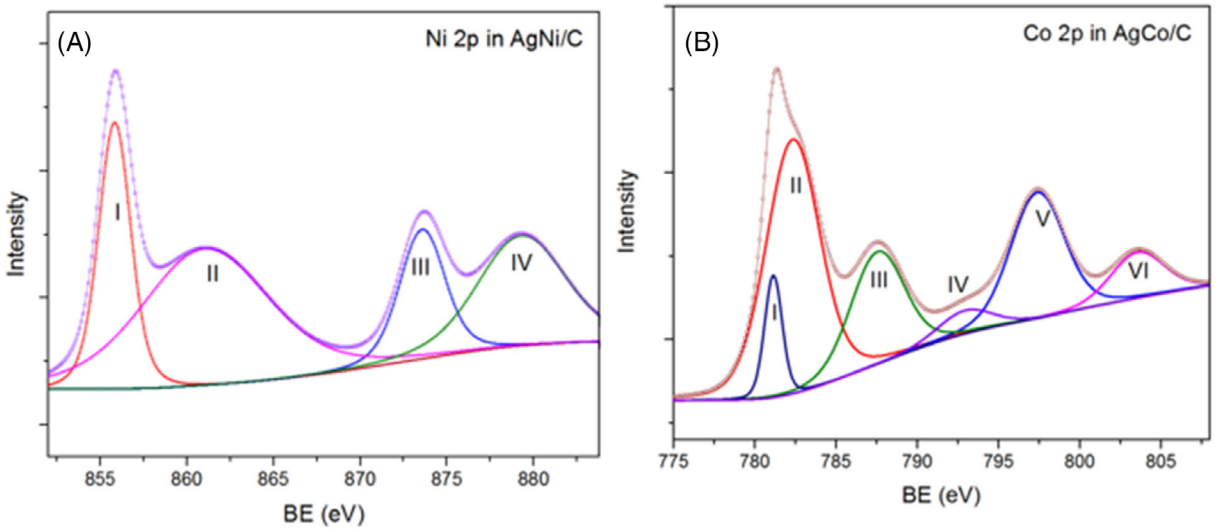

FIGURE 6 X-ray photoelectron spectroscopic spectrum at (A) Ni-2p edge for AgNi/C, and (B) Co 2p edge for AgCo/C

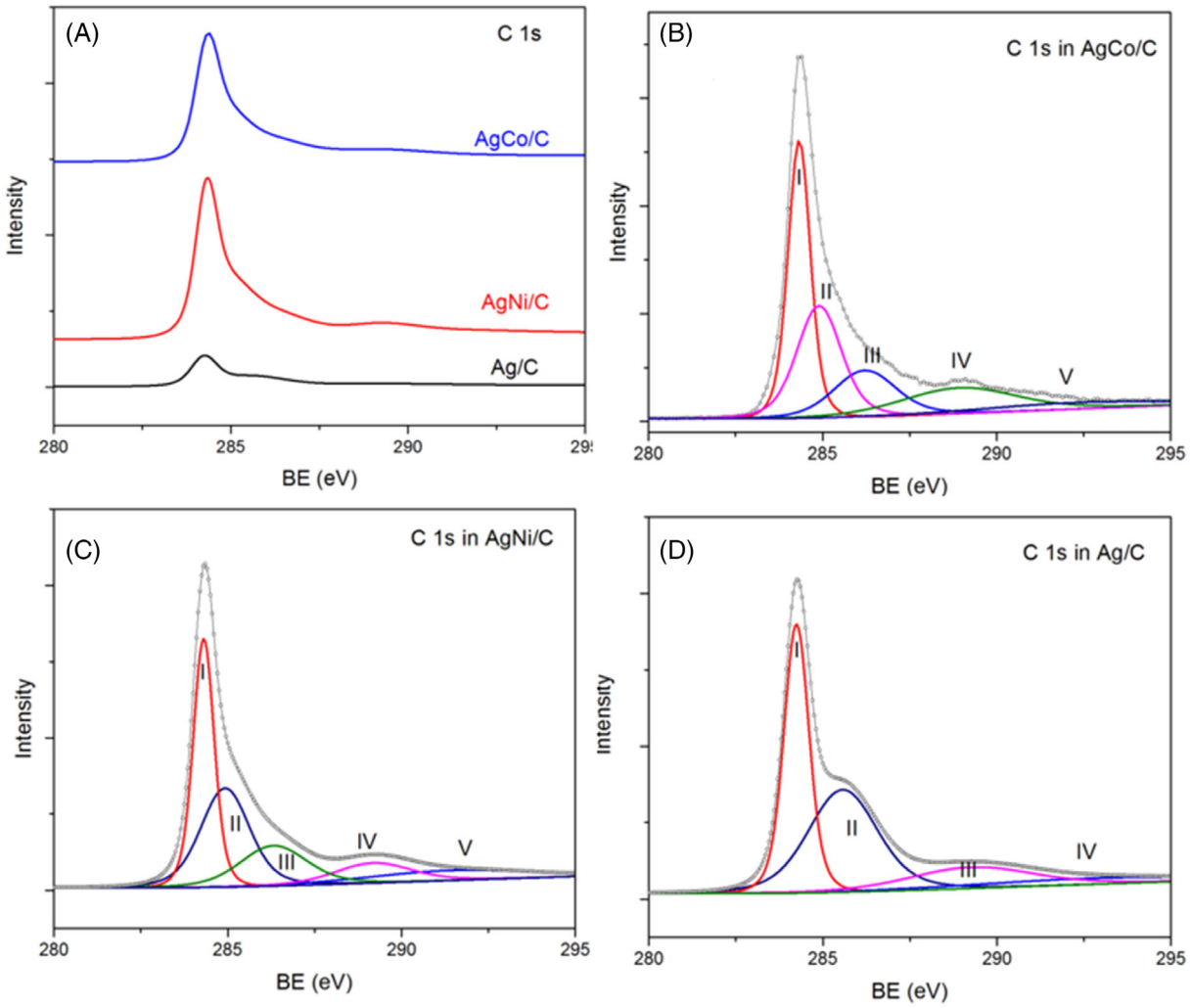

FIGURE 7 X-ray photoelectron spectroscopic spectrum at C 1s edge for (A) Ag/C, (B) AgCo/C, (C) AgNi/C (D)

that there are silver nanoparticles that do not form alloys. Observing the EXAFS regions shown in Figure 8B, the bond distances are almost the same as that of bulk silver (2.89 Å). There is also a consistency in the EXAFS regions for the AgCo and AgNi with only silver-silver scattering in the nanoparticles and not much second metal scattering observed. The samples, however, do have considerable changes in coordination numbers as seen by the marked variations in the area of the peak in the first shell. Through the equation relating the coordination number and particle size developed for gold nanoparticles[51]; $\log(\%_{\text{dispersion}}) = -0.130N + 2.58$, in which N signifies the coordination number; the dispersion, and therefore the size (assuming the particles are spherical), can be calculated (see Table 1). It can be said that, based on the similarity of the results, silver nanoparticles that are not alloyed are present. The metal's identity corresponds with nanoparticles of varying sizes as shown in Table 1.

Combining the XPS and XAS analysis, it looks like there is only limited alloying between Ag-M (M = Ni, Co) that is restricted to the surface. This possibly could be a result of the synthesis technique employed in preparing the samples. Even though, all the metal precursors were introduced at the same time during synthesis, the differences in their decomposition temperatures and interactions with the reduction agents follow a sequential pattern. The Ni and Co metal nitrates decompose and react with the reducing agent to form Ni/Co nanoparticles, and subsequently silver nitrate decomposes and Ag(+1) reduces to Ag(0) to form silver clusters on the surface of already synthesized Ni or Co particles, resulting in a surface restricted alloying.[43] The XPS analysis indicates changes in the Ag oxidation states, and confirms some degree of alloying on the surface.

3.1 | Electrochemical analysis

Cyclic voltammetry (CV) was initially utilized to analyze the electrocatalytic activity of the bi-metallic AgNi/C and

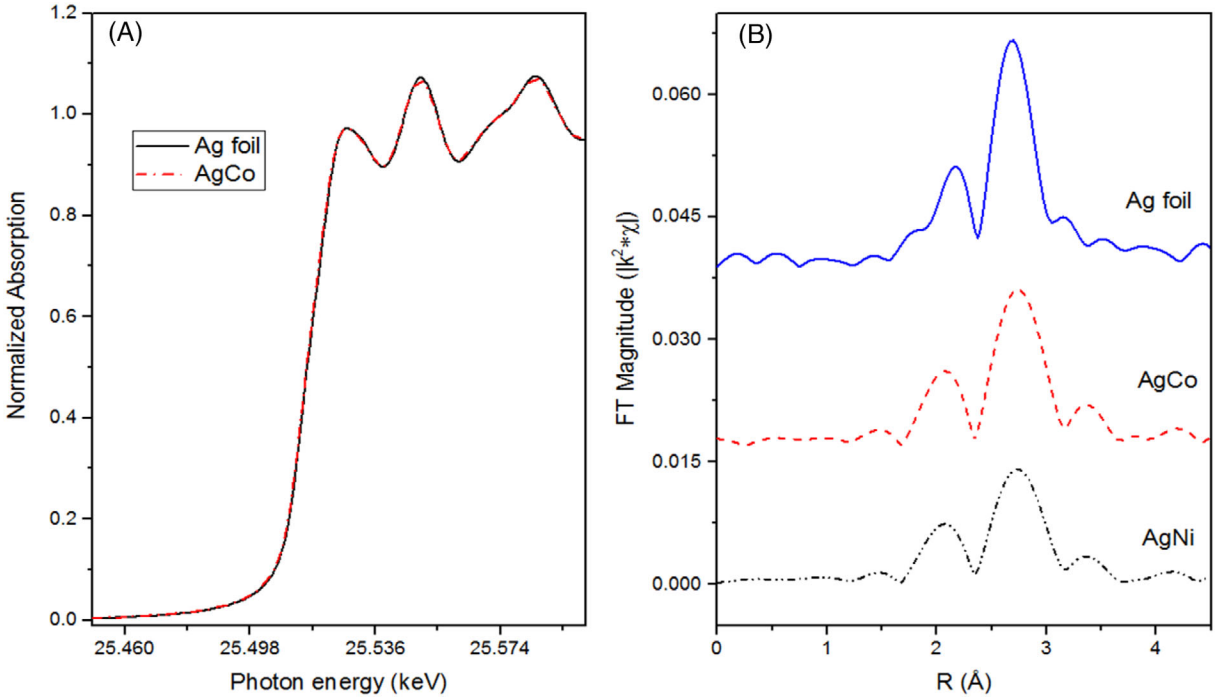

FIGURE 8 (A) XANES region of Ag foil and AgCo, and (B) EXAFS regions for bulk Ag, AgCo, and AgNi

TABLE 1 EXAFS fitting of Ag-metal nanoparticles

Sample	Edge energy (eV)	Ag-Ag CN	Bond distance (Å)	$\Delta\sigma^2$ [a,b]	ΔE_0 [b]	Particle size (nm)
Ag-foil	25 514.0	12.0[c]	2.89[c]	–	–	Bulk
AgCo	25 512.9	10.3	2.90	0.001	1.60	6
AgNi	25 513.2	7.5	2.90	0.001	0.87	2.5

[a]Fixed when fitting samples to avoid overfitting.
[b]Differences are calculated relative to the Ag-foil reference.
[c]Standard with known values fixed when fitting.

AgCo/C catalysts toward methanol electrooxidation in comparison to the electrocatalyst consisting of only silver supported on carbon. The performance of the electrocatalysts in a solution of 1 M KOH before methanol addition and in the presence of N_2 at 50 mV s^{-1} scan rate is shown in Figure 9. The increase in polarization from a value of −0.6 to +0.6 V was obtained in the anodic direction. Afterwards the applied potential was reversed and directed toward −0.6 V in the cathodic direction. The CV curve for Ag/C in Figure 9 displayed an upward (anodic) peak at around +0.27 V and a cathodic peak at approximately −0.01 V. AgCo/C, on the other hand, displayed an anodic peak at relatively greater potential of +0.29 V (and higher current density of ca. 2.02 mA cm^{-2}) and cathodic peaks at about −0.31, +0.03, and +0.35 V. The anodic peak of AgNi/C can be observed at a higher potential value than that of Ag/C and AgCo/C catalysts (ca. +0.40 V) and cathodic peaks at +0.05 and +0.27 V. Figure 10A shows the CV of AgCo/C, AgNi/C, and Ag/C in a solution of 1 M KOH in the presence of nitrogen and 1 M methanol at 10 mV s^{-1} scan rate. In the figure, it can be observed that the CV curve for Ag/C deposited on the glassy carbon electrode displayed an anodic peak at approximately +0.28 V and other small peaks at higher positive potential values, and a cathodic peak at approximately +0.03 V that could be ascribed to Ag_2O and AgO formation, and AgO and Ag_2O reduction in the mixture, respectively.[54,55] In comparison to the CV curve of Ag/C in a KOH solution without methanol, these potential values of anodic and cathodic peaks are slightly higher. The CV curves for AgNi/C and AgCo/C in a mixture of KOH and CH_3OH solution, besides, display their anodic peaks that signify silver oxide formation at approximately +0.3 V, but at lower current density values in comparison to that of Ag/C. Furthermore, the CV curves of AgNi/C and AgCo/C displayed cathodic peaks at ca. +0.07 and +0.06 V, respectively, that could also be attributed to the reduction of AgO and Ag_2O. When

comparing the CV curves of AgCo/C in the different solutions (with and without CH_3OH) the anodic peak is around the same value of approximately +0.3 V, however the current density is greater (about 2.05 mA cm^{-2}) in the solution wherein methanol is absent. Furthermore, there are 3 cathodic peaks displayed by AgCo/C in the solution without methanol (at around −0.31, +0.03, and +0.35 V) while only one cathodic peak was shown by the electrocatalyst in the solution in which methanol is present (at ca. +0.06 V). Observing the CV curves of AgNi/C in the two types of solutions the anodic peaks in the solution without methanol and with methanol were +0.40 and +0.30 V, respectively. Two cathodic peaks were noticed in the KOH solution without methanol (at about +0.05 and +0.27 V) while only a single cathodic peak was observed in the solution with methanol being present at around +0.07 V.

To better understand activity of the electrocatalysts for methanol oxidation reaction LSV measurements were also performed. Based on the anodic polarization curves in Figure 10B, the current densities increase for each electrocatalyst, however they have different onset potentials. A comparison of the anodic LSV polarization results indicates that AgNi/C performs relatively better (with a lower onset potential of 0.41 V) than AgCo/C (0.45 V onset potential) and Ag/C (0.59 V onset potential). However, at higher potential of 0.8 V onwards, the current density of AgNi/C (41.61 mA cm^{-2}) and AgCo/C (38.85 mA cm^{-2}) are closer, with AgNi/C still dominating, nonetheless both have better current density than Ag/C which is only 6.60 mA cm^{-2}, significantly lower than the Ag-M catalysts. The three catalysts were evaluated for their stability using chronoamperometry (CA) at 0.5 V for a duration of 20 h in a N_2-purged solution of 1 M KOH and 1 M CH_3OH. Figure 10C demonstrates that the current density of AgNi/C toward MOR is comparatively greater than AgCo/C and Ag/C, with Ag/C being the lowest among the three electrocatalysts. Furthermore, the decay in the current density of the CA curve for AgNi/C is not as rapid as that shown by the CA curves of AgCo/C and Ag/C, which further supports the relatively better performance of the AgNi/C catalysts for MOR. The rapid decay in potentiostatic current density displayed by AgCo/C and Ag/C could be attributed to the adsorption of reaction intermediates that are generated during the oxidation of methanol, oxygen and hydrogen species present in the electrolyte. Furthermore, from the figure it can be observed that AgNi/C is also capable of maintaining the highest activity among the three electrocatalysts during the entire duration of the CA test.

The proposed MOR mechanism taking place on the electrocatalysts is that methanol gets adsorbed on the surface of the catalyst to finally produce CO_2 after going through a number of complex reactions.[34] The electrons supplied through the glassy carbon electrode leads to the processes of proton and electron pair generation from the carbonaceous compound. Several adsorption and deprotonation steps take place that produce intermediate species, that further undergo transformative reactions. The water molecules surrounding the anode also generate

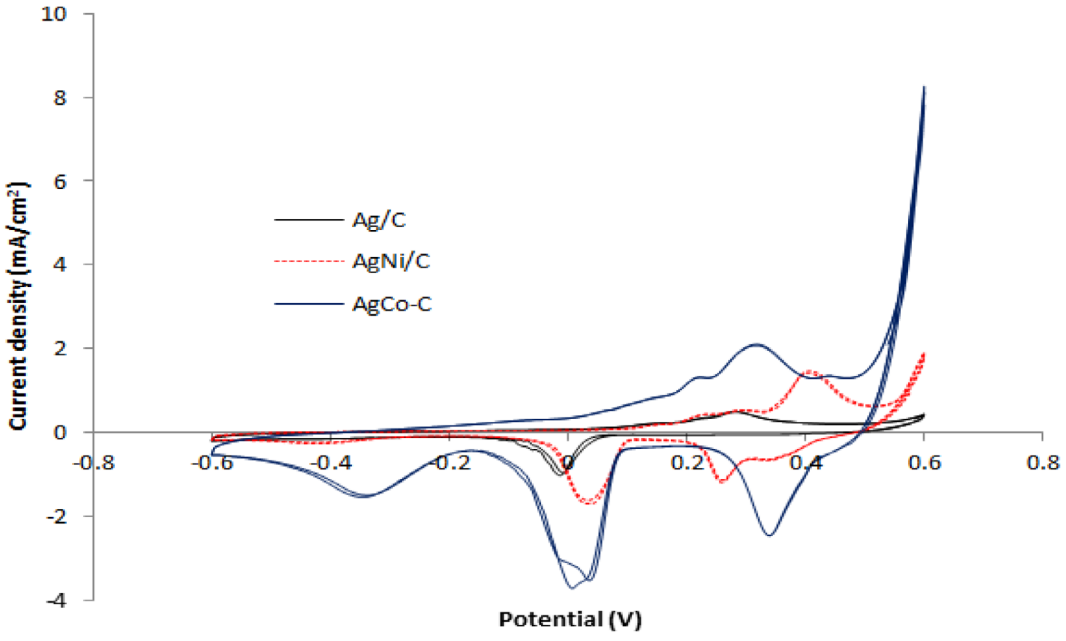

FIGURE 9 Cyclic voltammetry analysis to determine the performance of the electrocatalysts in 1 M KOH solution (saturated by N_2) before MeOH addition

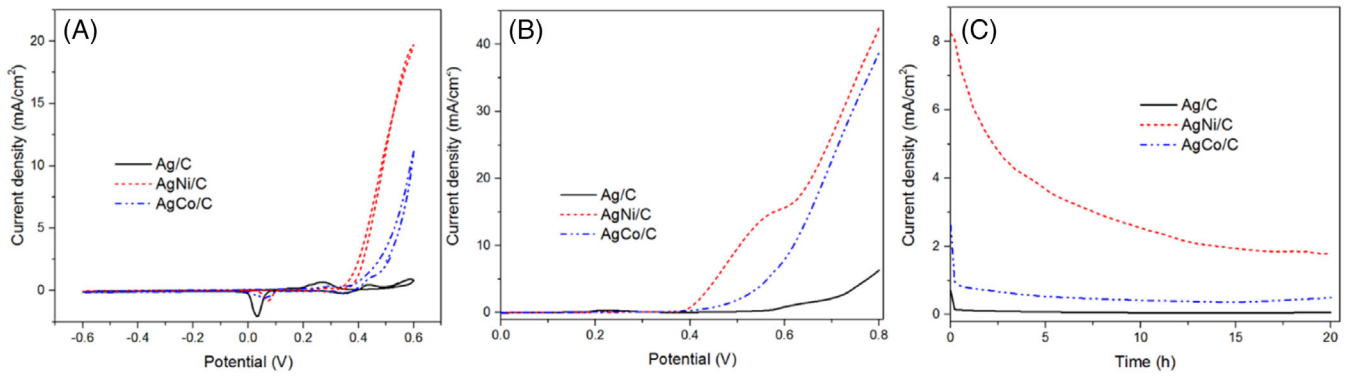

FIGURE 10 Methanol oxidation reaction electrocatalytic performance of catalysts, (A) cyclic voltammetry analysis, (B) linear sweep voltammetry analysis, and (C) chronoamperometry analysis

electron/proton pair as hydroxyl groups that combine with some of the surface intermediates. Among the intermediates, CO minimizes the rate of MOR in the anode because it has greater stability and its formation can cause the blockage of the electrocatalysts' active sites.[52,53] CO is formed due to an indirect mechanism where CHO or COH gets directly dehydrogenated. CO_2, on the other hand, is formed through hydroxyl group addition and several dehydrogenation processes. First, OH group is formed when formaldehyde or hydroxymethylene undergoes hydrogen abstraction resulting in formyl or COH, whereafter a proton/electron pair is extracted from a water molecule to produce the OH group. The group afterwards combines together with the carbonaceous species leading to the production of di-oxygenated species (eg, dihydroxycarbene [$C(OH)_2$] or formic acid [HCOOH]). Dehydrogenation then takes place to generate either carboxyl (COOH) or formate (HCOO) that then forms CO_2 after subsequent dehydrogenation. Alternatively, CO_2 production can be seen through a direct pathway wherein a proton/electron pair is extracted from water and the resulting hydroxyl that is produced is added to formaldehyde to form an intermediate H_2COOH. Dehydrogenation of this intermediate can cause formic acid or dioxymethylene (H_2COO) to be produced and with further dehydrogenation of dioxymethylene (first to formate) CO_2 is formed that gets desorbed from the electrocatalysts.

4 | CONCLUSIONS

The synthesis of three types of Ag-based electrocatalysts was performed using a solution combustion synthesis method. Results of XRD analysis showed the presence of graphitic carbon in carbon nanotubes in all the three electrocatalysts. Detailed analysis using XRD, XAS, and XPS indicate that the bulk of the electrocatalysts are not alloyed showing separate phases of silver and nickel/cobalt-oxides, whereas a surface alloying is confirmed indicating metals to be present in various oxidation states. The presence of well-porous structure on the surface of the electrocatalysts was confirmed by SEM micro images and the elemental phase distribution of silver in the electrocatalysts was determined from TEM analysis, especially the way by which Ag nanoparticles are distributed with nanoparticles of nickel (in AgNi/C) and cobalt (in AgCo/C), a characteristic that was further analyzed using XPS. The electrocatalytic performance of the Ag-M eletrocatalysts (AgNi/C and AgCo/C) was compared with Ag alone catalyst supported on carbon. Based on CV, LSV, and CA analysis, it was established that AgNi/C was the most active and stable catalyst in comparison to AgCo/C and Ag/C toward MOR. The AgNi/C demonstrated the highest current density with relatively slower decay among the three electrocatalysts when analyzed using CA, indicating its potential for long-term sustainable application in methanol oxidation.

ACKNOWLEDGEMENTS

This work was made possible by the NPRP grant (NPRP13S-0109-200029 and NPRP8-145-2-066) from the Qatar National Research Fund (a member of Qatar Foundation). The statements made herein are solely the responsibility of the authors. Use of the Advanced Photon Source is supported by the U.S. Department of Energy, Office of Science, and Office of Basic Energy Sciences, under contract DE-AC02-06CH11357. Authors would also like to acknowledge Dr. Md. Abdul Matin for his initial support on catalysts synthesis and characterization. The authors would also like to acknowledge QEERI Core Labs for their support related to the TEM characterization.

DATA AVAILABILITY STATEMENT

Data available in article.

REFERENCES

1. Heinzel A, Barragán VM. Review of the state-of-the-art of the methanol crossover in direct methanol fuel cells. *J Power Sources*. 1999;84:70-74. doi:10.1016/S0378-7753(99)00302-X
2. Eberle U, Müller B, Von Helmolt R. Fuel cell electric vehicles and hydrogen infrastructure: status 2012. *Energy Environ Sci*. 2012;5:8780-8798. doi:10.1039/c2ee22596d
3. Matin MA, Saad MAHS, Kumar A, Al-Marri MJ, Mansour SA. Effect of fuel content on the electrocatalytic methanol oxidation performance of Pt/ZnO nanoparticles synthesized by solution combustion. *Appl Surf Sci*. 2019;492:73-81. doi:10.1016/J.APSUSC.2019.06.213
4. Matin MA, Lee E, Kim H, Yoon WS, Kwon YU. Rational syntheses of core-shell Fe@(PtRu) nanoparticle electrocatalysts for the methanol oxidation reaction with complete suppression of CO-poisoning and highly enhanced activity. *J Mater Chem A*. 2015;3:17154-17164. doi:10.1039/c5ta03809j
5. Nassr ABAA, Bron M. Microwave-assisted ethanol reduction as a new method for the preparation of highly active and stable CNT-supported PtRu electrocatalysts for methanol oxidation. *ChemCatChem*. 2013;5:1472-1480. doi:10.1002/cctc.201200742
6. Meher SK, Rao GR. Polymer-assisted hydrothermal synthesis of highly reducible shuttle-shaped CeO_2: microstructural effect on promoting Pt/C for methanol electrooxidation. *ACS Catal*. 2012;2:2795-2809. doi:10.1021/cs300473e
7. Wang W, Huang Q, Liu J, Zou Z, Li Z, Yang H. One-step synthesis of carbon-supported Pd-Pt alloy electrocatalysts for methanol tolerant oxygen reduction. *Electrochem Commun*. 2008;10:1396-1399. doi:10.1016/j.elecom.2008.07.018
8. Jiang X, Gür TM, Prinz FB, Bent SF. Sputtered Pt–Ru alloys as catalysts for highly concentrated methanol oxidation. *J Electrochem Soc*. 2010;157:B314. doi:10.1149/1.3273081
9. Eid K, Ahmad YH, AlQaradawi SY, Allam NK. Rational design of porous binary Pt-based nanodendrites as efficient catalysts for direct glucose fuel cells over a wide pH range. *Catal Sci Technol*. 2017;7:2819-2827. doi:10.1039/c7cy00860k
10. Liu Z, Ling XY, Guo B, Hong L, Lee JY. Pt and PtRu nanoparticles deposited on single-wall carbon nanotubes for methanol electro-oxidation. *J Power Sources*. 2007;167:272-280. doi:10.1016/j.jpowsour.2007.02.044
11. Gao L, Yue W, Tao S, Fan L. Novel strategy for preparation of graphene-Pd, Pt composite, and its enhanced electrocatalytic activity for alcohol oxidation. *Langmuir*. 2013;29:957-964. doi:10.1021/la303663x
12. Zhao H, Yu C, You H, et al. A green chemical approach for preparation of Pt xCu y nanoparticles with a concave surface in molten salt for methanol and formic acid oxidation reactions. *J Mater Chem*. 2012;22:4780-4789. doi:10.1039/c2jm15792f
13. Shaik F, Zhang W, Niu W, Lu X. Volume-confined synthesis of ligand-free gold nanoparticles with tailored sizes for enhanced catalytic activity. *Chem Phys Lett*. 2014;613:95-99. doi:10.1016/j.cplett.2014.08.005
14. Chatenet M, Genies-Bultel L, Aurousseau M, Durand R, Andolfatto F. Oxygen reduction on silver catalysts in solutions containing various concentrations of sodium hydroxide—comparison with platinum. *J Appl Electrochem*. 2002;32:1131-1140. doi:10.1023/A:1021231503922
15. Rai T, Panda D. An extracellular enzyme synthesizes narrow-sized silver nanoparticles in both water and methanol. *Chem Phys Lett*. 2015;623:108-112. doi:10.1016/j.cplett.2015.02.003
16. Matin MA, Kumar A, Bhosale RR, Saleh Saad MAH, Almomani FA, Al-Marri MJ. PdZn nanoparticle electrocatalysts synthesized by solution combustion for methanol oxidation reaction in an alkaline medium. *RSC Adv*. 2017;7:42709-42717. doi:10.1039/c7ra07013f
17. Kang Y, Xue Q, Jin P, Jiang J, Zeng J, Chen Y. Rhodium nanosheets-reduced graphene oxide hybrids: a highly active platinum-alternative electrocatalyst for the methanol oxidation reaction in alkaline media. *ACS Sustain Chem Eng*. 2017;5:10156-10162. doi:10.1021/acssuschemeng.7b02163
18. Wu S, Liu J, Tian Z, et al. Highly dispersed ultrafine Pt nanoparticles on reduced graphene oxide nanosheets: In situ sacrificial template synthesis and superior electrocatalytic performance for methanol oxidation. *ACS Appl Mater Interfaces*. 2015;7:22935-22940. doi:10.1021/acsami.5b06153
19. Krissanasaeranee M, Wongkasemjit S, Cheetham AK, Eder D. Complex carbon nanotube-inorganic hybrid materials as next-generation photocatalysts. *Chem Phys Lett*. 2010;496:133-138. doi:10.1016/j.cplett.2010.07.043
20. Shearer CJ, Cherevan A, Eder D. Application and future challenges of functional nanocarbon hybrids. *Adv Mater*. 2014;26:2295-2318. doi:10.1002/adma.201305254
21. Yuda A, Kumar A. A review of g-C_3N_4 based catalysts for direct methanol fuel cells. *Int J Hydrogen Energy*. 2021;47:3371-3395. doi:10.1016/J.IJHYDENE.2021.01.080
22. Lazarov D, Manev S, Ivanov K. Oxidation of methanol on the surfaces of copper-silver alloys. *Mater Chem*. 1982;7:331-346. doi:10.1016/0390-6035(82)90013-X
23. Nazir R, Kumar A, Ali Saleh Saad M, Ali S. Development of CuAg/Cu_2O nanoparticles on carbon nitride surface for methanol oxidation and selective conversion of carbon dioxide into formate. *J Colloid Interface Sci*. 2020;578:726-737. doi:10.1016/J.JCIS.2020.06.033
24. Antonietta Casadei M, Pletcher D. The influence of conditions on the electrocatalytic hydrogenation of organic molecules. *Electrochim Acta*. 1988;33:117-120. doi:10.1016/0013-4686(88)80042-2
25. Raj IA, Vasu KI. Transition metal-based hydrogen electrodes in alkaline solution—electrocatalysis on nickel based binary alloy coatings. *J Appl Electrochem*. 1990;20:32-38. doi:10.1007/BF01012468
26. Fan C, Piron DL, Sleb A, Paradis P. Study of electrodeposited nickel-molybdenum, nickel-tungsten, cobalt-molybdenum, and cobalt-tungsten as hydrogen electrodes in alkaline water electrolysis. *J Electrochem Soc*. 1994;141:382-387. doi:10.1149/1.2054736
27. Wen T-C, Lin S-M, Tsai J-M. Sulphur content and the hydrogen evolving activity of NiS_x deposits using statistical experimental strategies. *J Appl Electrochem*. 1994;24:233-238.
28. Fleischmann M, Korinek K, Pletcher D. The oxidation of organic compounds at a nickel anode in alkaline solution. *J Electroanal Chem*. 1971;31:39-49. doi:10.1016/S0022-0728(71)80040-2
29. Taraszewska J, Rosłonek G. Electrocatalytic oxidation of methanol on a glassy carbon electrode modified by nickel hydroxide formed by ex situ chemical precipitation. *J Electroanal Chem*. 1994;364:209-213. doi:10.1016/0022-0728(93)02919-9
30. Allen JR, Florido A, Young SD, Daunert S, Bachas LG. Nitrite-selective electrode based on an electropolymerized cobalt phthalocyanine. *Electroanalysis*. 1995;7:710-713. doi:10.1002/elan.1140070803

31. Bettelheim A, White BA, Raybuck SA, Murray RW. Electrochemical polymerization of amino-, pyrrole-, and hydroxy-substituted tetraphenylporphyrins. *Inorg Chem*. 1987;26:1009-1017. doi:10.1021/ic00254a011
32. Macor KA, Spiro TG. Porphyrin electrode films prepared by electrooxidation of metalloprotoporphyrins. *J Am Chem Soc*. 1983;105:5601-5607. doi:10.1021/ja00355a012
33. Van Effen RM, Evans DH. A study of aldehyde oxidation at glassy carbon, mercury, copper, silver, gold and nickel anodes. *J Electroanal Chem*. 1979;103:383-397. doi:10.1016/S0022-0728(79)80362-9
34. Yuda A, Ashok A, Kumar A. A comprehensive and critical review on recent progress in anode catalyst for methanol oxidation reaction. *Sci Eng*. 2020;64:126-228. doi:10.1080/01614940.2020.1802811
35. Qiu H, Zou F. Nanoporous PtCo surface alloy architecture with enhanced properties for methanol electrooxidation. *ACS Appl Mater Interfaces*. 2012;4:1404-1410. doi:10.1021/AM201659N
36. Amin RS, El-Khatib KM, Hameed RMA, Souaya ER, Etman MA. Synthesis of Pt–Co nanoparticles on multi-walled carbon nanotubes for methanol oxidation in H_2SO_4 solution. *Appl Catal A Gen*. 2011;407:195-203. doi:10.1016/j.apcata.2011.08.045
37. Hidai S, Kobayashi M, Niwa H, et al. Changes in electronic states of platinum–cobalt alloy catalyst for polymer electrolyte fuel cells by potential cycling. *J Power Sources*. 2011;196:8340-8345. doi:10.1016/J.JPOWSOUR.2011.06.054
38. Ashok A, Kumar A, Yuda A, Al Ashraf A. Highly efficient methanol oxidation reaction on durable Co9S8@N,S-doped CNT catalyst for methanol fuel cell applications. *Int J Hydrogen Energy*. 2021;47:3346-3357. doi:10.1016/J.IJHYDENE.2021.07.026
39. Nazir R, Khalfani A, Abdelfattah O, Kumar A, Saad MAS, Ali S. Nanosheet synthesis of mixed Co_3O_4/CuO via combustion method for methanol oxidation and carbon dioxide reduction. *Langmuir*. 2020;36:12760-12771. doi:10.1021/ACS.LANGMUIR.0C02554
40. Sun Z, Talreja N, Tao H, et al. Catalysis of carbon dioxide photoreduction on nanosheets: fundamentals and challenges. *Angew Chemie Int Ed*. 2018;57:7610-7627. doi:10.1002/ANIE.201710509
41. Ashok A, Kumar A, Matin MA, Tarlochan F. Synthesis of highly efficient bifunctional Ag/Co_3O_4 catalyst for oxygen reduction and oxygen evolution reactions in alkaline medium. *ACS Omega*. 2018;3:7745-7756. doi:10.1021/ACSOMEGA.8B00799
42. Chen Y, Zheng XX, Huang XY, et al. Trimetallic PtRhCo petal-assembled alloyed nanoflowers as efficient and stable bifunctional electrocatalyst for ethylene glycol oxidation and hydrogen evolution reactions. *J Colloid Interface Sci*. 2020;559:206-214. doi:10.1016/j.jcis.2019.10.024
43. Ashok A, Kumar A, Tarlochan F. Surface alloying in silver–cobalt through a second wave solution combustion synthesis technique. *Nanomater*. 2018;8:604. doi:10.3390/NANO8080604
44. Govindasamy M, Mani V, Chen S-M, Sathiyan A, Merlin JP, Boopathy G. Polyaniline/nickel composite film modified electrode for sensitive electrochemical determination of ascorbic acid. *Int J Electrochem Sci*. 2016;11:10806-10814. doi:10.20964/2016.12.98
45. Niu HJ, Zhang L, Feng JJ, Zhang QL, Huang H, Wang AJ. Graphene-encapsulated cobalt nanoparticles embedded in porous nitrogen-doped graphitic carbon nanosheets as efficient electrocatalysts for oxygen reduction reaction. *J Colloid Interface Sci*. 2019;552:744-751. doi:10.1016/j.jcis.2019.05.099
46. Joo Y, Ahmed MS, Han HS, Jeon S. Preparation of electrochemically reduced graphene oxide-based silver–cobalt alloy nanocatalysts for efficient oxygen reduction reaction. *Int J Hydrogen Energy*. 2017;42:21751-21761. doi:10.1016/j.ijhydene.2017.07.123
47. Zhang Z, Xin L, Sun K, Li W. Pd-Ni electrocatalysts for efficient ethanol oxidation reaction in alkaline electrolyte. *Int J Hydrogen Energy*. 2011;36:12686-12697. doi:10.1016/j.ijhydene.2011.06.141
48. Hernández-Rodríguez MA, Goya MC, Arévalo MC, Rodríguez JL, Pastor E. Carbon supported Ag and Ag–Co catalysts tolerant to methanol and ethanol for the oxygen reduction reaction in alkaline media. *Int J Hydrogen Energy*. 2016;41:19789-19798. doi:10.1016/j.ijhydene.2016.07.188
49. Wolf EE, Kumar A, Mukasyan AS. Combustion synthesis: a novel method of catalyst preparation. *Catalysis*. 2019;31:297-346. doi:10.1039/9781788016971-00297
50. Ashok A, Kumar A. Ag/Co_3O_4 as an effective catalyst for glycerol electro-oxidation in alkaline medium. *Int J Hydrogen Energy*. 2021;46:4788-4797. doi:10.1016/J.IJHYDENE.2020.04.118
51. Miller JT, Kropf AJ, Zha Y, et al. The effect of gold particle size on AuAu bond length and reactivity toward oxygen in supported catalysts. *J Catal*. 2006;240:222-234. doi:10.1016/J.JCAT.2006.04.004
52. Direct Methanol Fuel Cells—technology.matthey.com, (n.d.). https://technology.matthey.com/article/40/4/150-159/ (accessed August 14, 2022).
53. Dinh HN, Ren X, Garzon FH, Zelenay P, Gottesfeld S. Electrocatalysis in direct methanol fuel cells: in-situ probing of PtRu anode catalyst surfaces. *J Electroanal Chem*. 2000;491:222-233. doi:10.1016/S0022-0728(00)00271-0
54. Quan H, Park SU, Park J. Electrochemical oxidation of glucose on silver nanoparticle-modified composite electrodes. *Electrochim Acta*. 2010;55:2232-2237. doi:10.1016/J.ELECTACTA.2009.11.074
55. Orozco G, Pérez MC, Rincón A, Gutiérrez C. Electrooxidation of methanol on silver in alkaline medium. *J Electroanal Chem*. 2000;495:71-78. doi:10.1016/S0022-0728(00)00396-X

How to cite this article: Yuda A, Kumar A, Abu Reesh I, et al. Electrooxidation of methanol on Ag, AgNi, and AgCo catalysts prepared by combustion synthesis technique. *Int J Energy Res*. 2022;1-14. doi:10.1002/er.8696